Atomistic investigations of polymer-doxorubicin-CNT compatibility for targeted cancer treatment

A molecular dynamics study

Kamath, Agneya; Laha, Anindita; Pandiyan, Sudharsan; Aswath, Surabhi; Vatti, Anoop Kishore; Dey, Poulumi

DOI
10.1016/j.molliq.2021.118005

Publication date
2022

Document Version
Final published version

Published in
Journal of Molecular Liquids

Journal of Molecular Liquids 348 (2022) 118005

Contents lists available at ScienceDirect

Journal of Molecular Liquids

journal homepage: www.elsevier.com/locate/molliq

Atomistic investigations of polymer-doxorubicin-CNT compatibility for targeted cancer treatment: A molecular dynamics study

Agneya Kamath [a], Anindita Laha [a], Sudharsan Pandiyan [b], Surabhi Aswath [a], Anoop Kishore Vatti [a,*], Poulumi Dey [c,*]

[a] Department of Chemical Engineering, Manipal Institute of Technology(MIT), Manipal Academy of Higher Education (MAHE), Manipal, Karnataka 576104, India
[b] Schrödinger, Bengaluru, Karnataka 560086, India
[c] Department of Materials Science and Engineering, Faculty of Mechanical, Maritime and Materials Engineering, Delft University of Technology, 2628 CD Delft, the Netherlands

ARTICLE INFO

Article history:
Received 6 August 2021
Revised 26 October 2021
Accepted 29 October 2021
Available online 9 November 2021

Keywords:
Doxorubicin
Anti-cancer Drug
Targeted Drug Delivery
Solubility Parameter
Molecular Dynamics

ABSTRACT

Doxorubicin is cytotoxic anthracycline antibiotic drug used in cancer treatment. The drug's efficacy in various kinds of cancer made its usage dominant for treating cancers. In this study, we determined the solubility of the doxorubicin in three different polymers, i.e., poly (N-isopropyl acrylamide), polyethylene glycol, and polyvinyl pyrrolidone, to increase the doxorubicin's drug efficacy on the targeted tumor site. We investigated the doxorubicin-polymer interactions with carbon-nanotube in the aqueous environment for the targeted delivery application using classical molecular dynamics simulations. An in-depth atomistic insight into polymer interaction with the drug/carbon-nanotube/water is obtained within the study. We have critically analyzed various properties such as interaction energy, hydrogen bonds between polymer-drug and polymer-water, the diffusion coefficient of the drug, end-to-end distance, radius of gyration of the polymer chains, and finally, drug density contours for different drug to polymer ratios. Our results explain the selection of effective monomer chain length of polymer and the suitability of the polymer carrier with doxorubicin.

1. Introduction

Doxorubicin (DOX) is an anti-cancer drug that is a non-selective class I anthracyclines antibiotics which is a savior drug for cancer treatment [1]. It has been used in various cancer treatments, including gastric, lung, bladder, ovarian, thyroid, soft tissue cancer, and breast cancer [2–4]. However, DOX is not exceptional; like any other anti-cancer drug, it causes several side effects on healthy cells. The probable reason is its high penetration capability through tissues and intercalating/binding properties with DNA, proteins with a function in the DNA replication are substantially ubiquitinated [5] and the ceasing of RNA transcription. Among various side effects, cardiotoxicity is the most predominant cytotoxicity of DOX [6,7]. The other common side effects of DOX include baldness, gastrointestinal problems, nausea, and disturbance to the neurological systems, and it also causes hallucination, and light-headedness [1,8,9]. It is known to cause nephropathy and proteinuria by injuring glomerular podocytes [10]. Additionally, DOX also exhibits anti-proliferation properties of cells, which helps to stop the growth of the cancer cells but causes enormous damage to healthy cells. This leads to suppression of the body's immune system [11–14]. To overcome these problems, the necessity for designing a targeted drug delivery system for cancer treatment is a need of the hour. In this regard, nanotechnology has emerged and showed promising applications in biomedical field [15–20].

Recently, carbon-nanotube (CNT) has attracted attention in the field of targeted drug-delivery applications [21,22]. CNTs are wrapped graphene sheets of hexagonally arranged sp^2 hybridized carbon atoms. Single wall and multiwall CNTs are used extensively to design targeted drug delivery systems [23]. Nano drug carriers carry a unique feature of enhanced performance and retention over the targeted tumor in cancer diseases due to their nanostructure. The ability of functionalized CNTs to release drug contents at the specific targeted site has substantially improved cancer treatment. The advantage of CNT-based targeted drug delivery is that it can deliver a very low dosage of the drug with minimal side effects. CNT provides an isolated environment to the drug, which prevents the degradation of the drug [24].

Despite of the several advantages, the application of CNT is limited because of its hydrophobic nature. The drug carrier design becomes very challenging because of the aggregation of the

* Corresponding authors.
E-mail addresses: anoop.vatti@manipal.edu (A.K. Vatti), P.Dey@tudelft.nl (P. Dey).

https://doi.org/10.1016/j.molliq.2021.118005
0167-7322/

hydrophobic CNT, which leads to undesirable toxicity such as cell-cycle arrest, apoptosis, and necrosis [19]. However, CNT functionalization with hydrophilic polymers improves the biocompatibility and stabilizes the carrier [25]. Therefore, the functionalization of the CNTs is necessary. CNTs can be functionalized with various polymers such as poly-N-isopropyl acrylamide (PNIPAM) [26,27], polyvinyl pyrrolidone (PVP) [28], poly(acrylic acid) (PAA) [29] and polyethylene glycol (PEG), and many others. While polymers such as polyacrylamide, polyethylene glycol, polymethacrylate, and polyvinyl amide are temperature-responsive, the poly acryl acids are pH-responsive [30].

Several experimental and theoretical investigations have been reported on DOX along with different polymers and nano carriers. Habibi et al. [28] synthesized two magnetic nanoparticles coated co-polymers that are PNIPAM and PVP. They performed experiments with this co-polymer nanomaterial for the delivery of the DOX drug. Their findings showed that high drug loading and low release time, along with magnetic properties, make these two composites suitable for the targeted drug delivery systems. Mina et al. [31] studied the DOX drug delivery with pristine graphene and graphene oxide as the nanocarriers using molecular dynamics (MD) simulations. The pH of the medium and surface oxidation density are considered as the principal parameters. The authors investigated the adsorption and release of the drug at neutral and acidic mediums. The study showed that neutral pH is favorable for the adsorption of the drug on the carrier, and at acidic pH, the drug releases from the surface of the carrier. Earlier theoretical investigations have proven that the functionalized CNTs adsorb more of the drug molecules than the pristine CNTs due to the excellent interaction between the drug molecules and the CNT's surface in the former case as mentioned before. The DOX is readily adsorbed on the surface of the CNTs via non-covalent π-π stacking [30]. Izadyar et al. [32] investigated the functionalization of CNT with the carboxylic group and studied the interaction of functionalized CNT with DOX in aqueous solution. It is concluded from the study that the adsorption behavior of DOX on CNTs is more accurately predicted by the Langmuir model than the Freundlich model.

Dimitrios Missirlis et al. [33] investigated the polymeric nanoparticles composed of poly(ethylene glycol) and poloxamer 407 (Pluronic F127). These polymeric nanoparticles were prepared via inverse emulsion photo-polymerization. Pluronic F127 is a symmetric triblock copolymer of poly(ethylene glycol)-bl-poly (propylene glycol)-bl-poly(ethylene glycol) (PEG-PPG-PEG). The DOX is encapsulated in PPG-rich hydrophobic areas, which are surrounded by a hydrophilic PEG-rich matrix of the nano-sized 3D polymeric hydrogel. The drug showed stability against hydrolytic degradation and continued to release DOX from the nanoparticulate system. Xia Dong et al. [34] investigated DOX-loaded hydrogel with four-arm PEG-PCL co-polymer along with porphyrin (POR). POR is a special fluorescent compound. Their results showed long-lasting therapeutic effects, as evident from the multispectral fluorescence imaging system. Min Liu et al. [35] developed the thermo-responsive co-polymer, alginate-g-poly(N-isopropyl acrylamide) (alginate-g-PNIPAAm), based stable injectable hydrogel. After the Alginate-g-PNIPAAm formed hydrogel, the polymer formed self-assembled micelles. These polymer matrices showed liquid soluble property below lower critical solution temperature (LCST) and became hydrogel when injected at the body temperature of 37°C. The hydrogel is encapsulated with the DOX. The DOX-encapsulated micelles showed enhanced permeability and retention effect. Further, a sustained and slow release of DOX is achieved without any sign of initial burst release.

Reza Maleki et al. [27] studied the effect of poly N-isopropyl acrylamide polymer chain length on the carbon-nanotube based drug delivery for the DOX drug using MD simulations. Their study concludes that the polymer with chain length, i.e., 15 mer is more stable and effective in drug delivery systems than the higher chain length polymer based on the structure and energetics of the system. Reza Maleki et al. [36] studied the pH-sensitive DOX release using single-walled and multi-walled CNTs. It is observed that the transportation and carrier properties are superior in multi-walled than single-walled CNTs. The interaction between multi-walled and DOX is observed to be strong. Further, the multi-walled system can release drugs slowly in comparison to the single-walled CNTs. Reza Maleki and co-workers [37] also performed MD simulations to study the effect of trimethyl chitosan as a functionalizing agent for fullerene to develop a smart and responsive drug delivery system. The investigators considered DOX and paclitaxel as the model anti-cancer drugs for the MD simulations to study the co-adsorption and co-release of the drug at neutral and acidic pH medium. The study concludes that the fullerene carrier is capable of adsorbing the DOX at neutral pH.

The existing works on the targeted drug delivery of DOX highlight several aspects as elaborated above. However, a systematic analysis and polymer screening for the DOX drug is still missing in the existing literature. The solubility parameter is an essential factor for selecting the suitable polymer for the drug and is considered as the main factor for designing a targeted drug delivery system. In this study, the solubility parameters for DOX and the selected polymers, i.e., PNIPAM, PVP, and PEG, are evaluated. Furthermore, an in-depth analysis of the end-to-end distance, the radius of gyration of the polymer chains, hydrogen bond interactions, and diffusion coefficient for the drug is presented. We also probed the density contour of the drug molecules at various drug concentrations within this work.

2. Computational Details

Latest Optimized Parameters for Liquid Simulations (OPLS4) [38] in Desmond [39] Molecular Dynamics package within Schrödinger simulation software [40] is used in this work. TIP3P water model is used for the solvent description. The anti-cancer drug is doxorubicin ($C_{27}H_{29}NO_{11}$), and three different polymers are PNIPAM, PEG, and PVP which we considered within our work. The considered system sizes are presented in Table 1. First, DOX molecules, polymers, and CNT are placed in the cubic box with an initial dimension of 50 Å. NPT equilibration simulation run is performed to achieve the equilibrated volume of the system in aqueous media, following which NVT simulations are performed.

The MD simulations are performed in NPT ensemble for a production run of 100 ns to calculate the solubility parameter for polymers. The time-step of 2 fs and temperature of 300 K are considered for the solubility parameter estimation simulations. We have considered 10 number of respective polymers to evaluate the solubility parameter. We have performed DOX conformational search using the mixed torsional and low mode sampling methods. This sampling method utilizes a combination of the random changes in torsion angles and molecular position. To evaluate the conformers that are dominant at room temperature, the Boltzmann population of a set of molecule structures is calculated. Based on the Boltzmann population, bulk doxorubicin molecules system is constructed to evaluate the bulk drug solubility parameter.

The doxorubicin, polymer, CNT and aqueous media simulation conditions are elaborated below. The MD simulations in the NPT ensemble are run for 25 ns, and later simulations in NVT ensemble are performed for a production run of 120 ns, which is analyzed. The temperature of 310 K approximately close to body temperature [41,42] is considered for simulations for the systems comprising of CNT, polymer and doxorubicin. Nose–Hoover chain thermostat and Martyna-Tobias-Klein barostat are used. The non-bonded interactions are truncated at 9 Å. We have considered 31

Table 1
The number of the drug molecules, polymers and CNTs used in simulation boxes are presented below. All the simulation boxes are filled with TIP3P water molecules.

Drug concentration (%)	Doxorubicin molecules	Polymer	Number of polymer chains	Repeat units	CNT
31	5	PNIPAM	5	15	1
31	5	PEG	13	15	1
31	5	PVP	5	15	1
50	10	PNIPAM	7	15	1
50	10	PEG	16	15	1
50	10	PVP	7	15	1

% and 50 % drug concentrations, and the drug concentration is evaluated using the following Eq. 1.

$$Drug\ Concentration = \frac{mass\ of\ drug}{mass\ of\ polymer} \times 100 \quad (1)$$

A single CNT is considered in the simulation box. The atomistic structure of the system comprising of the drug, PNIPAM, and CNT in an aqueous solution for 31 % of the drug concentration is shown in Fig. 1.

3. Results and Discussion

3.1. Solubility Parameter

The selected polymers are subjected to energy minimization and then MD simulation are performed in NPT ensemble to evaluate the Hildebrand solubility parameter. The Hildebrand solubility parameter and the heat of vaporization are closely related properties. The solubility parameter in $MPa^{1/2}$ is calculated using Eq. 2 which provides an estimate of the miscibility of drug and its polymer carrier. Despite the limitations of this approach, solubility parameters can provide a simple way for the rational selection of polymer carriers. Greenhalgh and co-workers [43] proposed that the solubility parameter difference between the polymer and drug ($\Delta\delta$) plays an important role in selecting the polymer carrier. Experiments showed that $\Delta\delta$ values between 1.6 to 7.5 $MPa^{1/2}$ are considered miscible. The polymer-drug system with $\Delta\delta$ values between 7.5 to 15 $MPa^{1/2}$ are slightly immiscible, whereas the $\Delta\delta >$ 15.9 $MPa^{1/2}$ are immiscible.

In this work, the solubility parameter is calculated for the drug and polymers for different monomer lengths. The evaluated solubility parameters for different number of repeating units of the polymer are summarized in the Table 2 for PNIPAM, Table 3 for PEG and Table 4 for PVP. The polymer and the bulk drug solubility parameter (δ) is evaluated using Eq. 2.

Table 2
The calculated solubility parameter for the different monomer length of the PNIPAM polymer and classification in terms of miscibility (i.e. $\Delta\delta$) for the polymer are presented below. The time series standard deviation σ is shown in parenthesis.

δ for DOX ($MPa^{1/2}$)	PNIPAM Monomers	δ for PNIPAM ($MPa^{1/2}$)	$\Delta\delta$ ($MPa^{1/2}$)
22.764 (0.127)	10	17.34 (0.23)	5.42
22.764 (0.127)	15	16.38 (0.19)	6.38
22.764 (0.127)	20	15.60 (0.21)	7.16
22.764 (0.127)	25	15.27 (0.18)	7.49
22.764 (0.127)	30	14.48 (0.31)	8.28
22.764 (0.127)	50	13.90 (0.26)	8.86

Table 3
The calculated solubility parameter for the different monomer length of the PEG polymer and classification in terms of miscibility (i.e. $\Delta\delta$) for the polymer are presented below. The time series standard deviation σ is shown in parenthesis.

δ for DOX ($MPa^{1/2}$)	PEG Monomers	δ for PEG ($MPa^{1/2}$)	$\Delta\delta$ ($MPa^{1/2}$)
22.764 (0.127)	10	23.57 (0.31)	0.81
22.764 (0.127)	15	22.16(0.18)	0.60
22.764 (0.127)	20	21.57 (0.18)	1.19
22.764 (0.127)	25	21.12(0.19)	1.64
22.764 (0.127)	30	20.84 (0.21)	1.92
22.764 (0.127)	50	19.83(0.13)	2.93

$$\delta = \sqrt{[(\Delta H_\vartheta / V_m)]} \quad (2)$$

where ΔH_ϑ is the heat of vaporization in kcal/mol and V_m is the molar volume.

The difference of the solubility parameters of the drug and polymer ($\Delta\delta$) can be seen in Table 2. It is noteworthy that the 10-mer, 15-mer and 20-mer are obtained to be miscible for PNIPAM within our study. As mentioned before, Reza et al. [27] showed that the PNIPAM 15-mer length is the most stable and effective in drug delivery systems. Table 3 shows the difference of the solubility

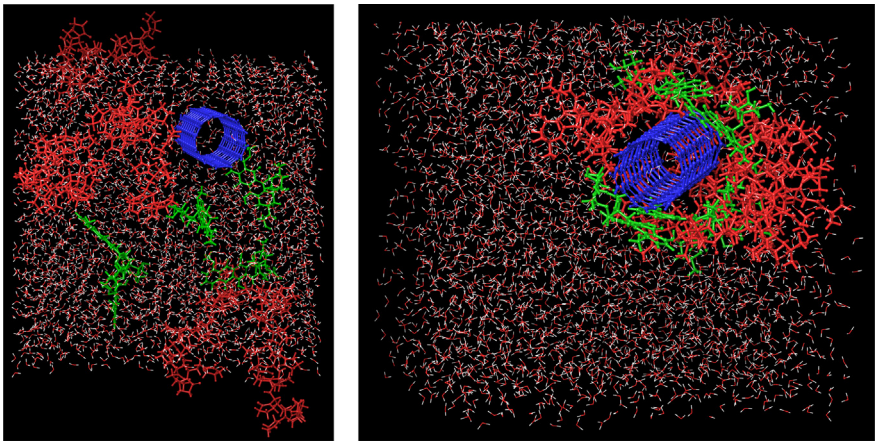

Fig. 1. A snapshot of doxorubicin (DOX), carbon-nanotube (CNT) and PNIPAM polymer in aqueous solution is shown. The following is the color coding: PNIPAM polymer (red), DOX (green), CNT (blue). The v-shaped markings are the water molecules. (Left) Before NPT simulation (Right) After NVT simulation at 43.65 ns.

Table 4
The calculated solubility parameter for the different monomer length of the PVP polymer and classification in terms of miscibility (i.e. $\Delta\delta$) for the polymer are presented below. The time series standard deviation σ is shown in parenthesis.

δ for DOX ($MPa^{1/2}$)	PVP Monomers	δ for PVP ($MPa^{1/2}$)	$\Delta\delta$ ($MPa^{1/2}$)
22.764 (0.127)	10	18.25 (0.19)	4.51
22.764 (0.127)	15	16.77 (0.12)	5.99
22.764 (0.127)	20	16.17(0.23)	6.59
22.764 (0.127)	25	15.58(0.22)	7.18
22.764 (0.127)	30	14.93(0.24)	7.83
22.764 (0.127)	50	14.71(0.13)	8.05

parameters for PEG at various monomer lengths. It can be seen based on the obtained difference in solubility parameter values that all the selected monomer lengths are suitable for the doxorubicin drug. Similarly, we probed the PVP as the polymer carrier for which the 10-mer, 15-mer, 20-mer and 25-mer PVP are obtained as suitable carriers for the doxorubicin drug as shown in Table 4. Based on our above analysis, we selected 15-mer polymer chain lengths for the PNIPAM, PVP, and PEG for performing MD simulations along with CNT in an aqueous solution.

3.2. Interaction Energy

We investigated the total interaction energy to understand the different pair interactions mainly doxorubicin-CNT, polymer-CNT and polymer-doxorubicin. The sum of the non-bonded interactions, mainly electrostatic and van der Waals (vdW) interaction energies yields the total interaction energy. The electrostatic and vdW interaction energies evaluated for different pairs of molecules are summarized in Table 5. The negative interaction energies with respect to the doxorubicin-CNT pair suggest that the attractive interactions dominate between DOX-CNT at drug concentrations considered within this study. The vdW interaction energies between PNIPAM-CNT, PEG-CNT and PVP-CNT are found to be −42.8107 kcal/mol, −3.1985 kcal/mol and −18.4593 kcal/mol respectively at 31% drug concentration. Based on the total interaction energies, PNIPAM polymer is found to be most attractive to the CNT at 31% drug concentration. The dominant vdW interaction energies are found for PNIPAM-CNT and PVP-CNT in comparison to the PEG-CNT. This attractive energy for the PNIPAM and PVP allows the higher aggregation of polymers around the CNT. It is interesting to note that for PNIPAM-DOX, PEG-DOX and PVP-DOX based on the total interaction energy, the PVP-DOX is the most attractive at 31% drug concentration in comparison to PNIPAM and PEG polymers. Our results indicate that there is strong vdW interaction between the PVP-DOX.

The vdW interaction energies between PNIPAM-CNT, PEG-CNT and PVP-CNT are found to be −0.0959 kcal/mol, −2.742 kcal/mol and −30.718 kcal/mol respectively at 50% drug concentration. Based on the total interaction energies, PVP polymer is found to be most attractive to the CNT at 50% drug concentration. The most dominant vdW interaction energy is found for PVP-CNT in comparison to PNIPAM-CNT and PEG-CNT. Overall, DOX-CNT is found to be attractive at 31% and 50% drug concentrations. Although, all the considered polymers are observed to be attractive to CNT, our results show that PNIPAM-CNT and PVP-CNT are the most attractive at 31% and at 50% drug concentrations respectively.

3.3. End-to-End Distance

The end-to-end distance of the polymer, i.e., the distance between one end of the polymer chain to the other end, is a critical quantity to probe the statistical measure of the polymer chains. The end-to-end distance is calculated using the worm-like chain model [44] for the semi-flexible side chains [45]. The end-to-end distance of the polymers averaged over all polymer molecules in system is calculated over the complete MD simulation production run using the following Eq. 3 [45]:

$$\left\langle h^2 \right\rangle = 2L_P L_0[1 - (L_P/L_0)(1 - exp(-L_0/L_P))] \quad (3)$$

where $\left\langle h^2 \right\rangle$ is the mean squared end-to-end distance, L_0 is the extended chain length, and L_P is the persistence length.

Table 6 summarizes the end-to-end distances along with the extended chain lengths and persistence lengths for the two different drug concentrations under consideration. The end-to-end distances for the three polymers are illustrated in Fig. 2 (a), (b) and (c) as a function of time for 31% drug concentration. It is evident from the figure that the end-to-end distances are 25.13 Å, 19.98 Å and 23.2 Å for PNIPAM, PEG and PVP respectively at 31% drug concentration. We also observed that the end-to-end distances at 50% drug concentration for all the considered polymers are inline with the 31% drug concentration. The persistence length indicates that there will be no correlation beyond this distance, i.e., the polymer chains are stiffer for a large distance. It can be seen from the values presented in Table 6 that there is a slight decrease in the persistence length with an increase in the drug concentration. The flexible chains enhance the polymer and drug interactions. Our study shows that polymer chain arrangement influences the drug interactions with the polymer based on the drug concentration. This is because flexible chains can interact with the higher amount of the drug at the 50% drug concentration.

Table 5
The average interaction energies between doxorubicin-CNT, polymer-CNT and polymer-doxorubicin are presented below.

Interaction Pair	doxorubicin-CNT		polymer-CNT		polymer-doxorubicin	
	Electrostatic	van der Waals	Electrostatic	van der Waals	Electrostatic	van der Waals
			31% drug concentration			
Interaction Energy (kcal/mol) (PNIPAM)	−0.6664	−30.1328	-0.6941	−42.8107	−0.4468	−1.9593
Total Interaction Energy (kcal/mol)	-30.799		-43.505		-2.406	
Interaction Energy (kcal/mol) (PEG)	−0.317	−25.3869	−0.0172	−3.1985	−0.6106	−1.5124
Total Interaction Energy (kcal/mol)	-25.704		-3.216		-2.123	
Interaction Energy (kcal/mol)(PVP)	−0.8763	−23.8958	−0.7996	−18.4593	−4.3851	−15.7169
Total Interaction Energy (kcal/mol)	-24.772		-19.259		-20.102	
			50% drug concentration			
Interaction Energy (kcal/mol) (PNIPAM)	−0.4874	−32.0421	−0.0172	−0.0959	0.0368	−0.0879
Total Interaction Energy (kcal/mol)	-32.530		-0.113		-0.051	
Interaction Energy (kcal/mol)(PEG)	−0.7203	−23.9811	−0.1905	−2.7422	−0.0926	−0.3097
Total Interaction Energy (kcal/mol)	-24.701		-2.933		-0.402	
Interaction Energy (kcal/mol) (PVP)	−0.1935	−25.0977	−0.1329	−30.7188	−5.3834	−0.0199
Total Interaction Energy (kcal/mol)	-25.291		-30.852		-5.403	

Table 6
The calculated end-to-end distance averaged over selected polymer chains over 120 ns of simulation time, persistence length, extended chain length (in Å) and the time series standard deviation (σ) corresponding to the end-to-end distance values are shown for drug-CNT-polymer system for different drug to polymer ratios.

Polymer	End-to-end distance (Å)	Persistence length (Å)	Extended chain length (Å)	σ (Å)
		31% drug concentration		
PNIPAM	25.13	8.60	46.53	2.02
PEG	19.98	4.41	56.30	1.78
PVP	23.22	7.77	44.84	2.11
		50% drug concentration		
PNIPAM	23.67	7.54	47.02	1.25
PEG	19.44	4.14	55.99	1.57
PVP	20.54	5.75	45.14	1.94

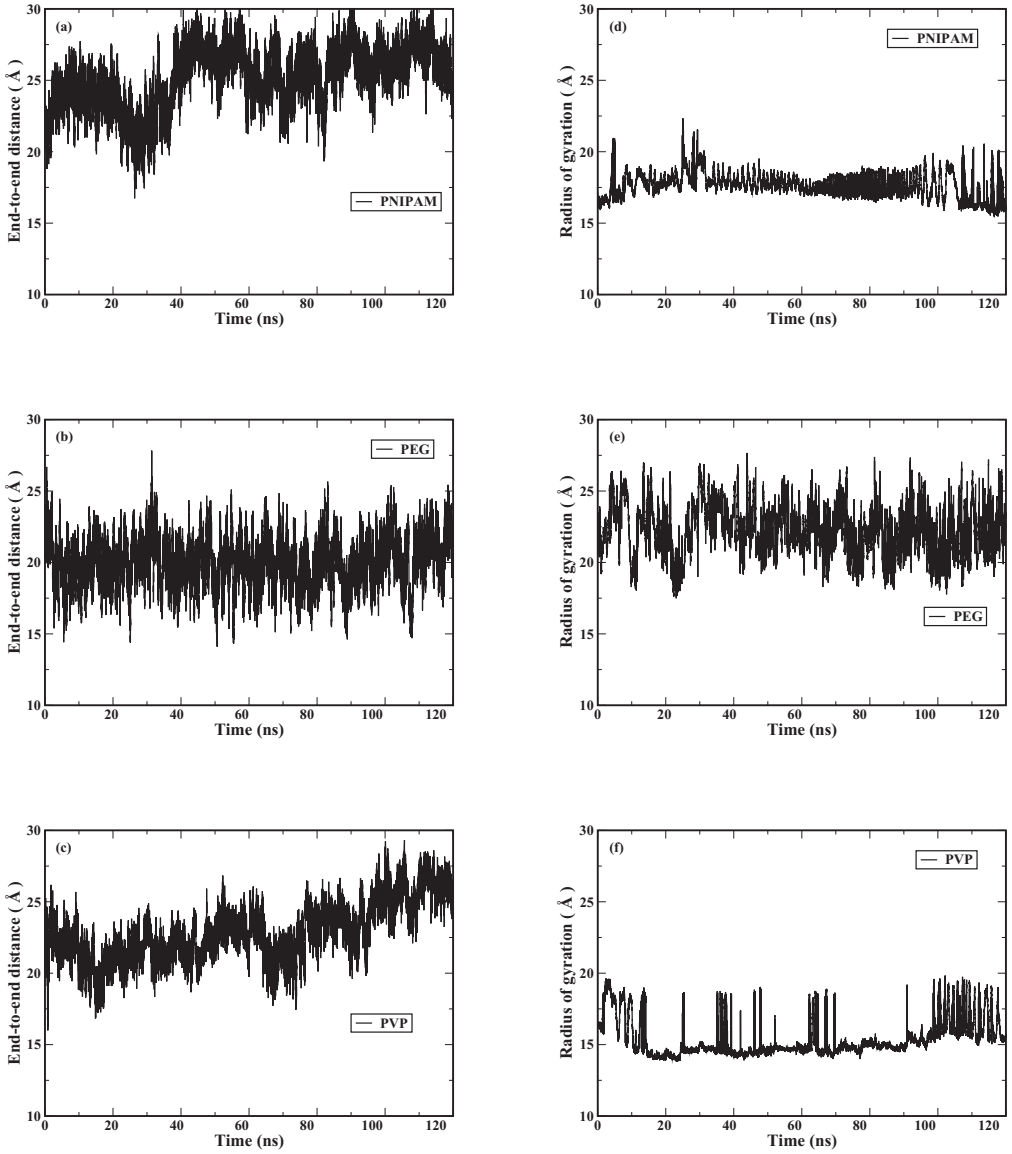

Fig. 2. End-to-end distances for polymers (a) PNIPAM (b) PEG and (c) PVP as a function of simulation time are shown. Radius of gyration for polymers (d) PNIPAM (e) PEG and (f) PVP plotted as a function of simulation time are shown. Calculations are performed at 31% drug concentration for 15mer.

3.4. Radius of Gyration

The radius of gyration intuitively allows to probe the size of the polymer coil. In our work, the radius of gyration of PNIPAM, PEG and PVP polymers are calculated. The radius of gyration (R_g) can be calculated using the following Eq. 4.

$$R_g = \sqrt{\frac{1}{N}\sum_{i=1}^{N}|r(i) - r_{centre}|^2} \tag{4}$$

where N is the total number of monomers, $r(i)$ and r_{centre} are the coordinates of a monomer i and the centre of mass, respectively.

R_g for polymer chains at the 31% and 50% concentrations are calculated and are presented in Table 7 for the selected polymers for drug compatibility. The calculated R_g as a function of time is shown in Fig. 2 (d), (e) and (f) at 31% drug concentration. The R_g values for the PNIPAM, PEG and PVP are found to be 17.42 Å, 22.19 Å and 15.68 Å, respectively. PEG, being hydrophilic and a linear molecule, is more flexible in comparison to the PNIPAM in aqueous solution. Higher radius of gyration signifies the higher dispersion of the drug molecules within the polymer matrix. Therefore, allowing the polymer to encapsulate the drug in a better way and to form a more stable complex. Interestingly, with an increase in the drug concentration, there is a slight increase in the R_g values. Overall, PEG polymer is found to have the highest value of R_g for both the considered drug concentrations.

3.5. Hydrogen Bonds

The hydrogen bond plays key role with respect to the interaction of the drug-polymer and polymer-water. Mainly, the better polymer-water interactions promote hydrophilicity nature of the polymer. The hydrogen bonds between two pairs are calculated, i.e., drug-polymer and polymer–solvent within this study. Fig. 3 shows the variation of the hydrogen bond as a function of simulation time for PNIPAM-doxorubicin and PNIPAM-water at 31% drug concentration.

The average number of the hydrogen bonds are summarized in Table 8 for the polymer-water and polymer-DOX at different drug concentrations. Overall with an increase in the drug concentration, there is an increase in hydrogen bonds. The highest number of hydrogen bonds is observed for the PNIPAM-DOX pair, and the lowest is noticed for the PEG- DOX. This indicates that there is a strong interaction between DOX and PNIPAM which in turn can lead to the stability of the polymer carrier. In general, with an increase in the drug concentration, there is an increase in hydrogen bonds for polymer-water. The highest number of hydrogen bonds are formed for PEG-water, and the lowest is observed for the PVP-water. The lowest number of hydrogen bonds for PVP indicates a good aggregation of the polymer compared to the PNIPAM and PEG. It is interesting to note, based on ratio of polymer-DOX to polymer-Water, that the H-bond count for PNIPAM-DOX interactions is the highest, followed by PVP and PEG. This same observation is noticed for the two different drug concentrations considered in this work.

3.6. Diffusion Coefficient

The diffusion coefficient averaged over all the doxorubicin drug molecules is calculated using the following Eq. 5 [46]:

$$D = \frac{1}{6}\lim_{t\to\infty}\frac{d}{dt}\left\langle |\vec{r}(t) - \vec{r}(0)|^2 \right\rangle \quad (5)$$

Table 7
The calculated radius of gyration (in Å) for polymer chains along with the standard deviation (σ) for two different drug concentrations are presented below.

Polymer	Radius of gyration (Å)	σ (Å)
	31% drug concentration	
PNIPAM	17.42	1.06
PEG	22.19	1.76
PVP	15.68	1.43
	50% drug concentration	
PNIPAM	18.65	1.32
PEG	27.62	2.04
PVP	18.03	1.49

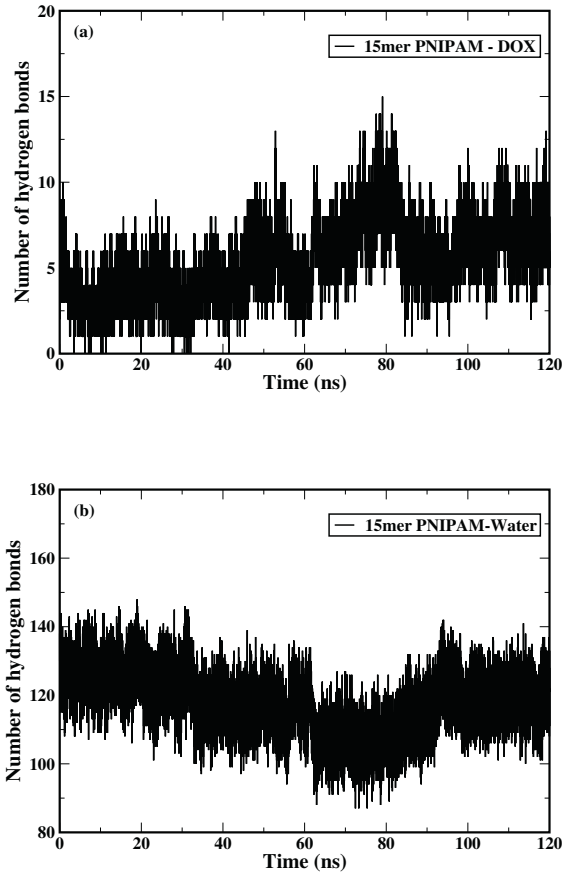

Fig. 3. The hydrogen bonds are shown for two different pairs namely (a) PNIPAM-Drug (b) PNIPAM-Water as a function of simulation time at 31% drug concentration.

Table 8
The calculated average number of hydrogen bonds are presented for selected polymer-water and polymer-DOX along with the ratio of polymer-DOX to polymer-Water for two different drug concentrations.

Polymer	Polymer-Water	Polymer-DOX	Ratio of polymer-DOX to polymer-water
	Average number of H-bonds		
	31% drug concentration		
PNIPAM	117	6	5.12 %
PEG	222	2	0.90 %
PVP	90	2	2.22 %
	50% drug concentration		
PNIPAM	160	13	8.12 %
PEG	280	3	1.07 %
PVP	115	4	3.47 %

$\left\langle |\vec{r}(t) - \vec{r}(0)|^2 \right\rangle$ is the mean-square displacement, where the angled brackets indicate an ensemble average, which is an average over all particles and time. The diffusion coefficients obtained within our study are presented in Table 9 for DOX present along with polymer and CNT in aqueous media. There is a clear sign that the diffusion coefficient depends strongly on the selected polymer. The highest diffusion coefficient is observed for the DOX in PVP polymer at 31% drug concentration. Further, with the increase in drug concentration, the diffusion coefficient of DOX is decreased due to the polymer's enhanced interactions except for the PEG. This is due to the fact that the PEG is hydrophilic and there is strong interaction between PEG-water as observed in our H-bonds calculations. This allows the higher mobility of drug molecules at higher drug concen-

Table 9
The calculated diffusion coefficients (in m^2/s) are shown for DOX molecule in three different polymer systems at the considered drug concentrations. The time series standard deviation (σ) is also presented.

Polymer	Doxorubicin diffusion coefficient (m^2/s) 31 % drug concentration	σ (m^2/s)
PNIPAM	4.69×10^{-11}	3.77×10^{-14}
PEG	3.56×10^{-11}	3.99×10^{-14}
PVP	7.77×10^{-11}	9.15×10^{-14}
	50 % drug concentration	
PNIPAM	1.85×10^{-11}	1.08×10^{-14}
PEG	11.8×10^{-11}	3.00×10^{-14}
PVP	4.24×10^{-11}	1.40×10^{-14}

trations. Our study reveals that a lower drug concentration plays a vital role in the higher mobility of the drug in polymer-carriers.

3.7. Drug Density Contours and Radial Distribution Function:DOX-CNT

The drug density cross-section contours are calculated by taking layers of a specified thickness perpendicular to a selected axis. The cross-section density is evaluated using the layer partitioned into cubes. The volume fraction of each atom that overlaps each cube is determined and weighted by the atomic mass, summed and divided by the cube volume to obtain the density in the cube.

The DOX densities at different concentrations are shown in Fig. 4. Fig. 4(a) and (b) show the drug density contours for the PNIPAM at both the drug concentrations, respectively. Likewise, Fig. 4 (c) and (d) shows the drug density contours for the PEG at both the drug concentrations, respectively. Finally, Fig. 4(e) and (f) shows the drug density contours for the PVP at both the drug concentrations, respectively. The dashed white box in the figures shows the average position of the CNT. It is evident from the figure that the drug molecules are slightly delocalized for the higher drug concentration. In contrast, for the lower drug concentration, drug molecules are localized around the CNT. We observed within our simulations that most of the drug molecules are attached to the CNT surface. Our results also indicate that although DOX density is delocalized, the highest concentration of the drug can be delivered at the targeted site using the CNTs.

Further, we probed the radial distribution function (RDF) for CNT-DOX in different polymer matrix. From the Fig. 5 (a) on RDF between CNT and DOX, a sharp peak around 8.8 Å can be seen, showing the average location of the DOX around CNT in the PEG matrix at 31% drug concentration. On the other hand, two peaks are observed at the 7.2 Å and 8.2 Å in the PNIPAM matrix. A broad peak is observed from 8.58 Å to 15 Å in the PVP matrix. The probability of finding the DOX in the vicinity of CNT is found to be highest in the PEG matrix than the PNIPAM and PVP matrix but DOX is close to CNT around 7.2 Å in the PNIPAM matrix. In Fig. 5 (b) at the 50% drug concentration, RDF sharp peak for the CNT-DOX is observed at 9.57 Å in the PVP matrix. Further, three peaks are

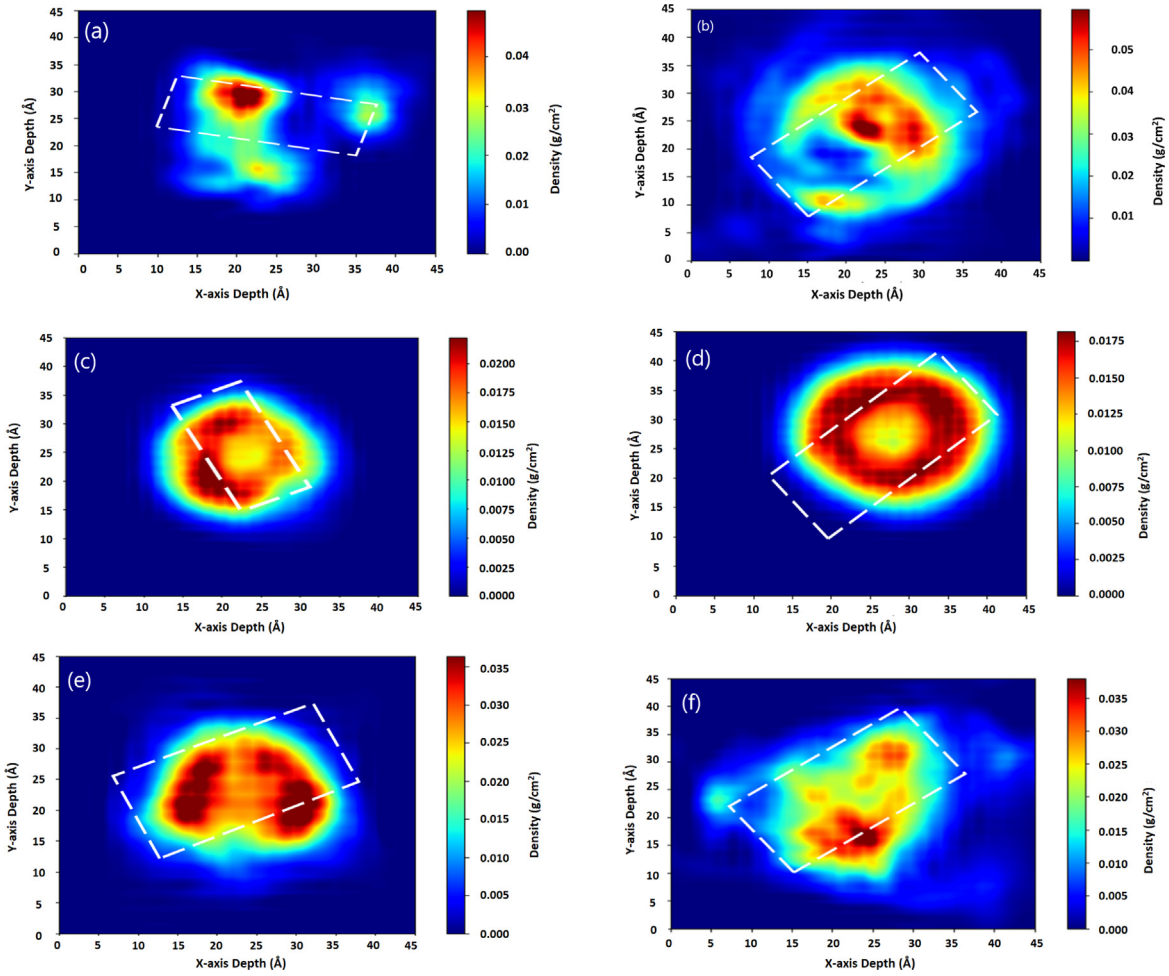

Fig. 4. Trajectory density contours of (a) Drug in PNIPAM (31% concentration) (b) Drug in PNIPAM (50% concentration) (c) Drug in PEG (31% concentration) (d) Drug in PEG (50% concentration) (e) Drug in PVP (31% concentration) (f) Drug in PVP (50% concentration). White dashed box shows the average position of the CNT.

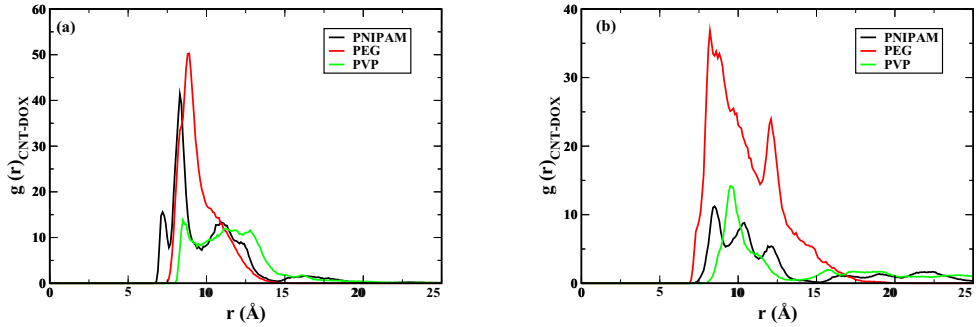

Fig. 5. (a) Radial distribution function between CNT and DOX at 31% drug concentration and (b) Radial distribution function between CNT and DOX at 50% drug concentration for polymers under consideration.

noticed for the CNT-DOX in PNIPAM matrix, starting from 8.15 Å to 14 Å. It is interesting to note that similar trends are observed for the PNIPAM at both the considered drug concentrations. The probability of finding the DOX is highest at 8.5 Å for 50% drug concentration within the PNIPAM matrix.

4. Conclusion

In this work, three different polymer-drug interactions are investigated by performing MD simulations at the various drug to polymer ratios. Interestingly, 15-mer polymer chain lengths of various polymers are found to be the best suitable for DOX-loaded drug carriers based on the solubility parameter results. The highest end-to-end distance is found for the PNIPAM in comparison to PEG and PVP. While investigating the radius of gyration (R_g) of various polymers, PEG polymer showed the highest value of the R_g in both the considered drug concentrations. This increase in R_g value suggests higher dispersion of the drug molecules within the polymer matrix. It is noteworthy that the diffusion coefficient of the DOX is observed to decrease inside the polymer matrix at the higher drug to polymer ratio except for the PEG. This discrepancy is due to the strong interactions between PEG and water, which in turn allows for the higher mobility of the DOX. It is seen that the highest diffusion coefficient is for the lower drug to polymer ratio thereby implying that a low drug concentration plays a vital role in the high mobility of the drug inside the polymer matrix. Additionally, PEG showed the highest number of hydrogen bonds with water among all the polymers investigated, promoting the polymer's hydrophilicity. We are of the opinion that the delocalized and localized drug density contours obtained within this study can be utilized for a better understanding of the drug distribution over the carbon-nanotube. To summarize, we believe that our study can be beneficial for the efficient and rationale drug design and for the targeted drug delivery applications for any kind of solid dispersed drugs keeping in view polymer-drug, polymer–solvent and drug-CNT interactions.

Declaration of Competing Interest

The authors declare that they have no known competing financial interests or personal relationships that could have appeared to influence the work reported in this paper.

Acknowledgments

The authors would like to thank Schrödinger Centre for Molecular Simulations, Manipal Academy of Higher Education (MAHE), Manipal for their support. Anindita Laha would like to thank Manipal Academy of Higher Education (MAHE), Manipal for research seed grant (reference number: 00000084). Fruitful discussions with Sriprasad Acharya is gratefully acknowledged.

References

[1] C. Carvalho, R.X. Santos, S. Cardoso, S. Correia, P.J. Oliveira, M.S. Santos, P.I. Moreira, Doxorubicin: the good, the bad and the ugly effect, Current medicinal chemistry 16 (25) (2009) 3267–3285.
[2] A. Jablonska Trypun, G. Swiderski, R. Kretowski, W. Lewandowski, Newly synthesized doxorubicin complexes with selected metals—synthesis, structure and anti-breast cancer activity, Molecules 22 (7) (2017) 1106.
[3] K.A. Cadoo, P.A. Kaufman, A.D. Seidman, C. Chang, D. Xing, T.A. Traina, Phase 2 study of dose-dense doxorubicin and cyclophosphamide followed by eribulin mesylate with or without prophylactic growth factor for adjuvant treatment of early-stage human epidermal growth factor receptor 2–negative breast cancer, Clinical breast cancer 18 (6) (2018) 433–440.
[4] B.L. Carroll, J. Bonica, A.A. Shamseddine, Y.A. Hannun, L.M. Obeid, A role for caspase-2 in sphingosine kinase 1 proteolysis in response to doxorubicin in breast cancer cells–implications for the chk 1-suppressed pathway, FEBS open bio 8 (1) (2018) 27–40.
[5] V.A. Halim, I. Garcia-Santisteban, D.O. Warmerdam, B. van den Broek, A.J. Heck, S. Mohammed, R.H. Medema, Doxorubicin-induced dna damage causes extensive ubiquitination of ribosomal proteins associated with a decrease in protein translation, Mol. Cell. Proteomics 17 (12) (2018) 2297–2308, URL https://www.sciencedirect.com/science/article/pii/S1535947620319952.
[6] Y. Sakata, J.-W. Dong, J.G. Vallejo, C.-H. Huang, J.S. Baker, K.J. Tracey, O. Tacheuchi, S. Akira, D.L. Mann, Toll-like receptor 2 modulates left ventricular function following ischemia-reperfusion injury, American Journal of Physiology-Heart and Circulatory Physiology 292 (1) (2007) H503–H509.
[7] R. Zilinyi, A. Czompa, A. Czegledi, A. Gajtko, D. Pituk, I. Lekli, A. Tosaki, The cardioprotective effect of metformin in doxorubicin-induced cardiotoxicity: the role of autophagy, Molecules 23 (5) (2018) 1184.
[8] G. Hortobágyi, Anthrazykline in der krebstherapie: Ein überblick, Drugs 54 (1997) 1–7.
[9] O. Tacar, P. Sriamornsak, C.R. Dass, Doxorubicin: an update on anticancer molecular action, toxicity and novel drug delivery systems, Journal of pharmacy and pharmacology 65 (2) (2013) 157–170.
[10] J. Cummings, C. McArdle, Studies on the in vivo disposition of adriamycin in human tumours which exhibit different responses to the drug, British journal of cancer 53 (6) (1986) 835.
[11] T. Kong, L. Hao, Y. Wei, X. Cai, B. Zhu, Doxorubicin conjugated carbon dots as a drug delivery system for human breast cancer therapy, Cell Prolif. 51 (5) (2018) e12488.
[12] M. Kumari, M.P. Purohit, S. Patnaik, Y. Shukla, P. Kumar, K.C. Gupta, Curcumin loaded selenium nanoparticles synergize the anticancer potential of doxorubicin contained in self-assembled, cell receptor targeted nanoparticles, Eur. J. Pharm. Biopharm. 130 (2018) 185–199.
[13] Nano-engineering of construction materials using molecular dynamics simulations: Prospects and challenges, Composites Part B: Engineering 143 (2018) 282 – 291.
[14] J. Pardo, Z. Peng, R.M. Leblanc, Cancer targeting and drug delivery using carbon-based quantum dots and nanotubes, Molecules 23 (2) (2018) 378.
[15] D.A. Gomez-Gualdron, J.C. Burgos, J. Yu, P.B. Balbuena, Carbon nanotubes: engineering biomedical applications, Progress in molecular biology and translational science, Vol. 104, Elsevier, 2011, pp. 175–245.
[16] C.D. Walkey, W.C. Chan, Understanding and controlling the interaction of nanomaterials with proteins in a physiological environment, Chem. Soc. Rev. 41 (7) (2012) 2780–2799.
[17] H. Song, J. Zhang, W. Wang, P. Huang, Y. Zhang, J. Liu, C. Li, D. Kong, Acid-responsive pegylated doxorubicin prodrug nanoparticles for neuropilin-1 receptor-mediated targeted drug delivery, Colloids Surf., B 136 (2015) 365–374.

[18] P. Pradeep, P. Kumar, Y.E. Choonara, V. Pillay, Targeted nanotechnologies for cancer intervention: a patent review (2010–2016), Expert opinion on therapeutic patents 27 (9) (2017) 1005–1019.
[19] H.J. Han, C. Ekweremadu, N. Patel, Advanced drug delivery system with nanomaterials for personalised medicine to treat breast cancer, Journal of Drug Delivery Science and Technology 52 (2019) 1051–1060.
[20] S. Mahajan, A. Patharkar, K. Kuche, R. Maheshwari, P.K. Deb, K. Kalia, R.K. Tekade, Functionalized carbon nanotubes as emerging delivery system for the treatment of cancer, International journal of pharmaceutics 548 (1) (2018) 540–558.
[21] S. Augustine, J. Singh, M. Srivastava, M. Sharma, A. Das, B.D. Malhotra, Recent advances in carbon based nanosystems for cancer theranostics, Biomaterials science 5 (5) (2017) 901–952.
[22] H. Liu, L. Zhang, M. Yan, J. Yu, Carbon nanostructures in biology and medicine, Journal of Materials Chemistry B 5 (32) (2017) 6437–6450.
[23] V. Rastogi, P. Yadav, S.S. Bhattacharya, A.K. Mishra, N. Verma, A. Verma, J.K. Pandit, Carbon nanotubes: an emerging drug carrier for targeting cancer cells, Journal of drug delivery (2014).
[24] A. Bianco, K. Kostarelos, e prato, m. applications of carbon nanotubes in drug delivery, Curr. Opin. Chem. Biol 9 (2005) 674–679.
[25] M. Roldo, D.G. Fatouros, Biomedical applications of carbon nanotubes, Annual Reports Section C(Physical Chemistry) 109 (2013) 10–35.
[26] X. Su, Y. Shuai, Z. Guo, Y. Feng, Functionalization of multi-walled carbon nanotubes with thermo-responsive azide-terminated poly (n-isopropylacrylamide) via click reactions, Molecules 18 (4) (2013) 4599–4612.
[27] R. Maleki, H.H. Afrouzi, M. Hosseini, D. Toghraie, S. Rostami, Molecular dynamics simulation of doxorubicin loading with n-isopropyl acrylamide carbon nanotube in a drug delivery system, Comput. Methods Programs Biomed. 184 (2020) 105303.
[28] D. Habibi, S. Kaamyabi, M.M. Amini, Doxorubicin poly n-vinylpyrrolidone and poly n-isopropylacrylamide-co-n-vinylpyrrolidone coated magnetic nanoparticles, Appl. Surf. Sci. 320 (2014) 301–308.
[29] A. Liu, I. Honma, M. Ichihara, H. Zhou, Poly (acrylic acid)-wrapped multi-walled carbon nanotubes composite solubilization in water: definitive spectroscopic properties, Nanotechnology 17 (12) (2006) 2845.
[30] M.N. Al-Qattan, P.K. Deb, R.K. Tekade, Molecular dynamics simulation strategies for designing carbon-nanotube-based targeted drug delivery, Drug Discovery Today 23 (2) (2018) 235–250.
[31] M. Mahdavi, F. Rahmani, S. Nouranian, Molecular simulation of ph-dependent diffusion, loading, and release of doxorubicin in graphene and graphene oxide drug delivery systems, Journal of Materials Chemistry B 4 (46) (2016) 7441–7451.
[32] A. Izadyar, N. Farhadian, N. Chenarani, Molecular dynamics simulation of doxorubicin adsorption on a bundle of functionalized cnt, J. Biomol. Struct. Dyn. 34 (8) (2016) 1797–1805.
[33] D. Missirlis, R. Kawamura, N. Tirelli, J.A. Hubbell, Doxorubicin encapsulation and diffusional release from stable, polymeric, hydrogel nanoparticles, Eur. J. Pharm. Sci. 29 (2) (2006) 120–129, URL https://www.sciencedirect.com/science/article/pii/S0928098706001680.
[34] X. Dong, H. Chen, J. Qin, C. Wei, J. Liang, T. Liu, D. Kong, F. Lv, Thermosensitive porphyrin-incorporated hydrogel with four-arm peg-pcl copolymer (ii): doxorubicin loaded hydrogel as a dual fluorescent drug delivery system for simultaneous imaging tracking in vivo, Drug Delivery 24 (1) (2017) 641–650, https://doi.org/10.1080/10717544.2017.1289570, pMID: 28282993.
[35] M. Liu, X. Song, Y. Wen, J.-L. Zhu, J. Li, Injectable thermoresponsive hydrogel formed by alginate-g-poly(n-isopropylacrylamide) that releases doxorubicin-encapsulated micelles as a smart drug delivery system, ACS Applied Materials & Interfaces 9 (41) (2017) 35673–35682, https://doi.org/10.1021/acsami.7b12849, pMID: 28937214.
[36] R. Maleki, H.H. Afrouzi, M. Hosseini, D. Toghraie, A. Piranfar, S. Rostami, ph-sensitive loading/releasing of doxorubicin using single-walled carbon nanotube and multi-walled carbon nanotube: A molecular dynamics study, Comput. Methods Programs Biomed. 186 (2020) 105210.
[37] R. Maleki, A. Khoshoei, E. Ghasemy, A. Rashidi, Molecular insight into the smart functionalized tmc-fullerene nanocarrier in the ph-responsive adsorption and release of anti-cancer drugs, J. Mol. Graph. Model. 100 (2020) 107660.
[38] C. Lu, C. Wu, D. Ghoreishi, W. Chen, L. Wang, W. Damm, G.A. Ross, M.K. Dahlgren, E. Russell, C.D. Von Bargen, R. Abel, R.A. Friesner, E.D. Harder, Opls 4: Improving force field accuracy on challenging regimes of chemical space, J. Chem. Theory Comput. 17 (7) (2021) 4291–4300, https://doi.org/10.1021/acs.jctc.1c00302, pMID: 34096718.
[39] K.J. Bowers, E. Chow, H. Xu, R.O. Dror, M.P. Eastwood, B.A. Gregersen, J.L. Klepeis, I. Kolossvary, M.A. Moraes, F.D. Sacerdoti, J.K. Salmon, Y. Shan, D.E. Shaw, Scalable algorithms for molecular dynamics simulations on commodity clusters, in: Proceedings of the 2006 ACM/IEEE Conference on Supercomputing, SC '06, ACM, New York, NY, USA, 2006.
[40] Schrödinger release 2018, in: Schrödinger Release 2018, Schrödinger, LLC, New York, NY, 2018.
[41] M. Karimi, P. Sahandi Zangabad, A. Ghasemi, M. Amiri, M. Bahrami, H. Malekzad, H. Ghahramanzadeh Asl, Z. Mahdieh, M. Bozorgomid, A. Ghasemi, M.R. Rahmani Taji Boyuk, M.R. Hamblin, Temperature-responsive smart nanocarriers for delivery of therapeutic agents: Applications and recent advances, ACS Applied Materials & Interfaces 8 (33) (2016) 21107–21133, https://doi.org/10.1021/acsami.6b00371, pMID: 27349465.
[42] Y.-J. Kim, Y.T. Matsunaga, Thermo-responsive polymers and their application as smart biomaterials, J. Mater. Chem. B 5 (2017) 4307–4321, https://doi.org/10.1039/C7TB00157F.
[43] D.J. Greenhalgh, A.C. Williams, P. Timmins, P. York, Solubility parameters as predictors of miscibility in solid dispersions, J. Pharm. Sci. 88 (11) (1999) 1182–1190.
[44] J.N. Milstein, J.-C. Meiners, Worm-like chain (wlc) model, in: Encyclopedia of Biophysics, Springer Berlin Heidelberg, Berlin, Heidelberg, 2013, pp. 2757–2760.
[45] S. Brinkers, H.R.C. Dietrich, F.H. de Groote, I.T. Young, B. Rieger, The persistence length of double stranded dna determined using dark field tethered particle motion, J. Chem. Phys. 130 (21) (2009) 215105.
[46] Understanding molecular simulation: From algorithms to applications, in: D. Frenkel, B. Smit (Eds.), Understanding Molecular Simulation (Second Edition), second edition Edition, Academic Press, San Diego, 2002.